铜铝异种金属激光焊接头组织特征及力学性能

薛志清[1,2]，　胡绳荪[1,2]，　左　迪[2]，　申俊琦[1,2]
(1. 天津大学 天津市现代连接技术重点实验室，天津　300072；2. 天津大学 材料科学与工程学院，天津　300072)

摘　要：铜铝异种金属薄板的激光焊加热和冷却速度快，焊缝区温度梯度和成分浓度梯度大，接头微观组织具有特殊性. 通过激光焊接试验、拉伸测试、焊缝横截面及断口 SEM 和 DES 分析，研究了铜铝薄板的激光搭接焊接头组织分布特征及其对性能的影响. 结果表明，在高温度梯度和浓度梯度下焊缝区形成了组织形貌不同的区域，分别是平行排列的板条状过共晶组织区、板条状过共晶组织与共晶组织混合区(简称混合区)、片层状的共晶区以及枝晶状的亚共晶区. 拉伸剪切断裂在混合区. 随着焊接速度的增加，混合区的宽度变窄，混合区的过共晶组织由等轴状向板条状转变，试件承受的最大剪切力随之增大.

关键词：激光焊；异种金属；微观组织；力学性能
中图分类号：TG456.7　　**文献标识码**：A　　**文章编号**：0253－360X(2013)10－0051－04

薛志清

0　序　　言

铜铝异种金属之间在物理性能方面存在很大的差异[1－3]，例如熔点、密度、导热、比热容等. 铜和铝的导热性良好，铜的热导率是铝的 1.67 倍[4]. 因此铜铝异种金属焊接过程中，无论是铜在上铝在下还是铝在上铜在下，铜和铝的温度分布均不同. 由于铝的熔点低于铜的熔点，且铜的热导率高于铝，所以铝在上铜在下搭接焊时，铝容易过热烧损，而铜却不容易受热熔化，很难形成搭接焊缝. 铜在上铝在下搭接焊时，铜受热后很快将热量传导给铝，且铜的熔点高于铝，因此铜和铝容易同时受热熔化形成良好的焊缝. 焊接时铜铝熔化形成熔池，在表面张力、重力以及浮力的共同作用下熔池液态金属铜铝发生流动，铜和铝相互混合. 由于焊接时间很短，铜铝混合不充分导致焊缝内部成分不均匀. 同时铜铝在焊接过程中易形成金属间化合物[5－7]，例如 Cu_2Al，Cu_2Al_3，CuAl 和 $CuAl_2$. 金属间化合物形态和分布会影响铜铝接头的力学性能[3,4－6,8].

激光焊具有能量密度高、焊接速度快和热影响区窄等特点[9]. 铜铝异种金属薄板激光焊接时，加热和冷却速度快，熔池温度梯度高. 由于加热和冷却时间短，熔池金属铜和铝来不及混合和扩散而形成成分浓度梯度高的铜铝焊缝区. 焊缝区将呈现不同的组织形貌及成分分布. 铜铝搭接激光焊时所形成的焊缝区组织形态、分布及其对接头力学性能的影响正是人们所关注的问题.

文中主要研究铜铝薄板激光搭接焊过程中接头在快速熔化和冷却条件下微观组织特征及其对力学性能的影响.

1　试验方法

铜铝激光搭接焊(铜在上、铝在下)试验采用固体激光器 Nd: YAG(JK2003SM)，纯氩气作为保护气体. 激光功率为 1 650 W，激光光束半径为 0.4 mm，保护气体流量为 25 L/min. 焊接速度分别采用 125，135，145 和 155 mm/s. 所用的材料为工业纯铝(1060)和纯铜(T2)，铜铝试样尺寸均为 100 mm × 20 mm × 0.3 mm. 激光焊接试验之前用砂纸对工件表面进行打磨，提高铜表面粗糙度，进而增加铜表面对激光的吸收率.

焊后沿工件横截面进行切样、打磨和抛光. 试样采用 keller 试剂进行腐蚀，腐蚀剂的体积分数为 1% HF，1.5% HCl，2.5% HNO_3，95 % H_2O. 铜铝接头微观组织和成分分布采用 SEM 和 EDS 进行分析. 工件的拉伸抗剪强度采用 CCS-44100 测试仪进行测试. 每组数据测试三次，然后取平均值. 断口形貌及成分分析采用 SEM 和 EDS.

收稿日期：2013－04－17
基金项目：国家自然科学基金资助项目(50975195)

2 试验结果及讨论

2.1 微观组织特征及成分分布

焊接速度为 135 mm/s 时,铜铝焊接接头横截面的光学微观组织形貌如图 1 所示.

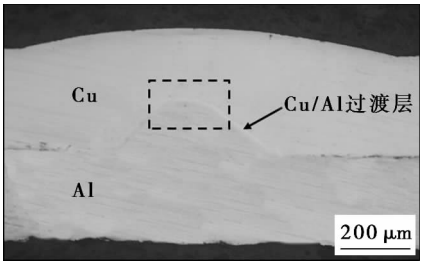

图 1 铜铝搭接接头横截面微观组织

Fig. 1 Optical image of Cu-Al lap cross-section

由图 1 可以看出,焊接过程中在表面张力、浮力、重力等的共同作用下,液态铝向铜流动并在铜板侧形成铜铝结合区. 虚线框部分结合区的 SEM 分析结果如图 2 所示.

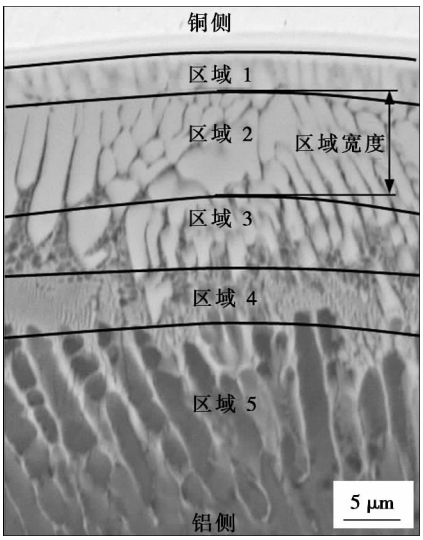

图 2 铜铝过渡区微观组织形貌

Fig. 2 Microstructure in Cu-Al intermediate layer

图 1 和图 2 均显示铜铝之间有明显的过渡层,类似于铜铝扩散焊接头过渡区[5]. 激光焊连续焊接时,功率密度为 3.28×10^5 W/cm^2,未达到匙孔焊的能量密度条件($\geqslant10^6$ W/cm^2) ,熔池金属没有发生充分的混合,而形成明显的铜铝过渡层. 根据组织形貌和成分可以将过渡区分为如图 2 所示的 5 个区域. 如图 2 所示,相邻区域边界之间的距离定义为该区域的宽度. 图 2 中不同区域的 SEM 放大如图 3 所示.

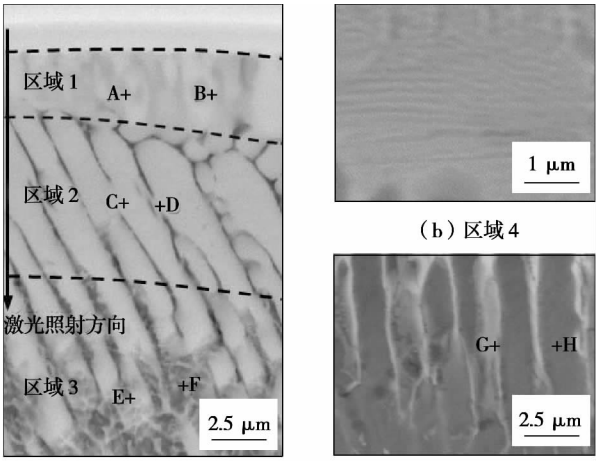

图 3 铜铝接头过渡区微观组织放大

Fig. 3 Microstructure of Cu-Al intermediate layer at high magnification

图 2 和图 3 中不同区域微观组织形貌特征以及相应的成分如表 1 所示.

表 1 铜铝结合区组织形貌及对应的成分

Table 1 Microstructure morphology and corresponding compositions of Cu-Al joint

区域	形貌特征	w_{Cu}(质量分数,%)	尺寸 d/μm
1	板条状组织,其轴平行于激光轴线	点 A: 68.79 点 B: 63.86	板条宽: 1.21 半条长: 3.88
2	板条状组织,其轴与激光轴线呈 30°夹角	点 C: 58.97 点 D: 55.03	板条宽: 1.53 板条长: 9.31
3	不连续板条状组织分布在网状组织中	点 E: 53.69 点 F: 34.72	板条宽: 1.43 板条长: 5.18
4	片层状组织	平均值: 33.86	层间距: 0.16 区域宽: 5.04
5	树枝状组织,一次枝晶相互平行	点 G: 15.73 点 H: 12.33	枝晶间距: 1.94 枝晶长度: 20.18

为了分析每个区域的组织及相,表 2 给出了 Cu-Al 二元合金固相及其对应的成分[8].

基于表 1 对铜铝接头微观组织形貌和成分的分析、表 2 铜 - 铝二元合金固相与铜质量分数的对应关系、铜 - 铝二元相图[10]以及以往对铜铝焊接所形成的合金金属间化合物的研究[5],可以推断出区域 1平行排列的板条状 CuAl 镶嵌在过固溶体中,区域 2 为 CuAl 和 $CuAl_2$ 的混合物镶嵌在过固溶体中,区域 3 为 $CuAl_2$ 不连续地分布在共晶组织中.

表 2　铜 - 铝二元合金固相及其所对应的成分

Table 2　Solid phases for Cu-Al system and their corresponding compositions

固相	w_{Cu}(质量分数,%)
Al	0.00 ~ 6.44
Al_2Cu	52.46 ~ 53.71
AlCu	70.03 ~ 72.09
Al_3Cu_4	74.37 ~ 75.21
Al_2Cu_3	77.44 ~ 79.28
Al_4Cu_9	79.70 ~ 83.98
Cu	90.57 ~ 100.00

区域 4 为片层状的共晶组织,其中 α-Al 和 θ 相交替平行排列成片层组织,片层组织的层间距为 0.16 μm,远小于定向凝固过程中形成的片层状组织(约为 1 μm). 区域 5 为树枝状亚共晶组织.

区域 1 和区域 2 均为板条状过共晶组织且平行排列. 因此把区域 1 和区域 2 统称为平行排列的板条状过共晶区. 虽然区域 3 类似于区域 2,但是区域 3 中的过共晶不连续地分布在共晶组织中. 因此把区域 3 称为过共晶组织与共晶组织的混合区,以下简称为混合区. 区域 2 和区域 3 中板条状组织取向与区域 1 不同,这是因为微观组织的取向与冷却过程中热量的传递方向有关[11].

2.2　铜铝接头拉伸剪切断口分析

对不同焊接速度 125,135,145 和 155 mm/s 条件(保持其它焊接条件不变)下的铜铝接头进行拉伸剪切试验. 断口表面进行 SEM 和 EDS 分析. 结果发现,在焊接速度 125 ~ 155 mm/s 范围内,接头均断裂在混合区(区域 3). 铜铝焊接接头断口形貌如图 4 所示.

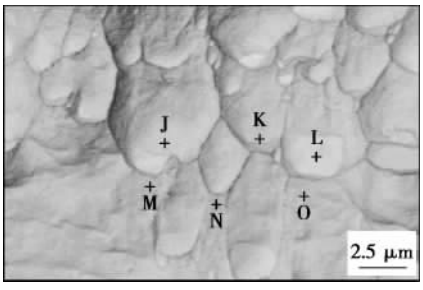

图 4　铜铝接头断口表面(铝侧)(v = 135 mm/s)

Fig. 4　Fracture surface of Cu-Al joint (Al side)

EDS 成分分析结果显示,点 J,K,L 处铜质量分数分别为 53.57%,54.03% 和 52.44%. 点 M,N,O 处铜质量分数分别为 34.64%,32.97% 和 34.14%. 由 2.1 节对铜铝固相及所对应的成分分析可知,J,K,L 处为金属间化合物 $CuAl_2$,M,N,O 处为共晶组织. 由此可见,拉伸剪切断裂发生在混合区. 不难看出,铜铝薄板激光搭接焊时,接头拉伸剪切薄弱点在于过共晶与共晶组织的混合区(区域 3).

2.3　焊接速度对微观组织及力学性能的影响

焊接速度变化时,铜铝接头组织随之变化,组织的改变会影响接头的最大剪切力. 图 5a 和图 5b 所示分别为混合区宽度和最大剪切力随焊接速度增加的变化曲线.

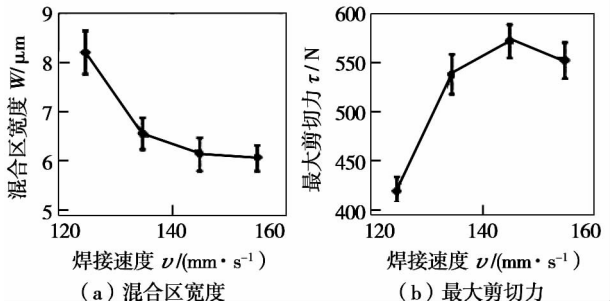

图 5　混合区宽度及最大剪切力随焊接速度的变化

Fig. 5　Variations of mixture zone width and maximum tensile stress with welding speed

由图 5a 和图 5b 可知,在焊接速度 125 ~ 145 mm/s范围内,混合区宽度随焊接速度增加而减小时,接头最大剪切力随焊接速度的增加而增大. 由此可见,混合区宽度的降低有助于接头最大剪切力的提高. 混合区(区域 3)组织随焊接速度的变化如图 6 所示. 可以看出随着焊接速度的增加,混合区组织由等轴状向板条状转变. 板条状组织固有的阻

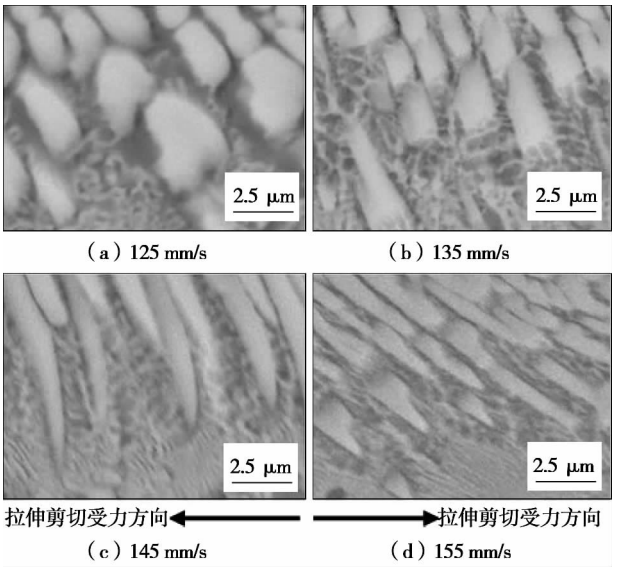

图 6　混合区组织随焊接速度的变化

Fig. 6　Variation of mixture zone microstructure with welding speed

止晶粒发生横向位移的能力,增加了接头区组织发生横向变形的阻力,因此铜铝搭接接头的拉伸剪切性能得以提高. 板条状组织纵轴与剪切力的夹角也会影响接头的最大拉伸剪切力,当板条状组织纵轴与拉伸剪切力方向夹角减小时(图 6d),板条状组织能承受的阻力减小,接头拉伸剪切力降低(图 5b). 焊接速度为 145 mm/s 时,铜铝搭接激光焊接头拉伸剪切力最高.

3 结 论

(1) 铜铝异种金属激光搭接焊接过程中,快速熔化和凝固导致熔池形成高的温度梯度和浓度梯度,使接头微观组织呈现明显的特征: 由板平行排列的板条状过共晶区、过共晶与共晶组织的混合区、片层状的共晶组织区以及枝晶状的亚共晶区组成.

(2) 拉伸剪切试验结果表明,断裂是发生在过共晶与共晶组织的混合区,该区域为拉伸剪切的薄弱区.

(3) 焊接速度增大时,混合区宽度减小,混合区的过共晶形态由等轴状向板条状转变,最大剪切力随之增大; 板条状过共晶组织有助于铜铝搭接接头最大剪切力的提高.

参考文献:

[1] Sun Z. Joining dissimilar material combinations: materials and processes [J]. International Journal of Materials and Product Technology, 1995, 10(1/2): 16 – 27.

[2] 张洪涛, 刘 多, 冯吉才, 等. 铝/铜高频感应接触反应钎焊[J]. 焊接学报, 2012, 33(3): 89 – 92.
Zhang Hongtao, Liu Duo, Feng Jicai, *et al*. Reactive contact brazing between aluminum alloy and copper by high frequency induction method [J]. Transactions of the China Welding Institution, 2012, 33(3): 89 – 92.

[3] 崔占全, 李 达, 孙明辉, 等. 7075 铝合金与 H68 黄铜的搅拌摩擦焊组织分析[J]. 焊接学报, 2011, 32(7): 91 – 94.
Cui Zhanquan, Li Da, Sun Minghui, *et al*. Microstructure of friction stir welding joint of 7075Al and H68 brass [J]. Transactions of the China Welding Institution, 2011, 32(7): 91 – 94.

[4] Mai T A, Spowage A C. Characterisation of dissimilar joints in laser welding of steel-kovar, copper-steel and copper-aluminum [J]. Materials Science and Engineering A, 2004, 374(1/2): 224 – 233.

[5] Abbasi M, Karimi Taheri A, Salehi M T. Growth rate of intermetallic compounds in Al/Cu bimetal produced by cold roll welding process [J]. Journal of Alloys and Compounds, 2001, 319(1/2): 233 – 241.

[6] Heideman R, Johnson C, Kou S. Metallurgical analysis of Al/Cu friction stir spot welding [J]. Science and Technology of Welding and Joining, 2010, 15(7): 597 – 604.

[7] 吴铭方, 司乃潮, 蒲 娟. 铝合金/铜/不锈钢接触反应钎焊[J]. 焊接学报, 2009, 30(11): 85 – 88.
Wu Mingfang, Si Naichao, Pu Juan. Contact reactive brazing between Al alloy/ Cu/ stainless steel and analysis on grain boundary penetration behaviors [J]. Transactions of the China Welding Institution, 2009, 30(11): 85 – 88.

[8] Guo Y J, Qiao G J, Jian W Z, *et al*. Microstructure and tensile behavior of Cu-Al multi-layered composites prepared by plasma activated sintering [J]. Materials Science and Engineering A, 2010, 527(20): 5234 – 5240.

[9] Sun Z, Ion J C. Laser welding of dissimilar metal combinations [J]. Journal of Materials Science, 1995, 30(17): 4205 – 4214.

[10] Massalski T B. Binary alloy phase diagrams volume 1 [M]. First Edition. Ohio: American Society for Metals, 1986.

[11] Gill S C, Kurz W. Laser rapid solidification of Al-Cu alloys: banded and plane front growth [J]. Materials Science and Engineering, 1993, 173(1/2): 335 – 338.

作者简介: 薛志清,男,1983 年出生,博士研究生. 主要从事铜铝异种金属的激光焊接工作. 发表论文 2 篇. Email: xuezq@tju.edu.cn

通讯作者: 申俊琦,男,讲师. Email: shenjunqi@tju.edu.cn

neering, Harbin Engineering University, Harbin 150001, China). pp 35 – 38

Abstract: Lap joints of 5A90 aluminium-lithium alloy were welded with refill friction spot welding process, in which the process parameters were changed for different purpose. The joint mechanical test of lap shear samples and cross tension samples, metallography analysis and joint microhardness test were carried out. The experimental results indicate that 1.5 mm thickness spot welded joint shear strength is more satisfying with tool rotation speed of 1 800 r/min and welding time of 1.5 s. The cross tension test results shows thats the joint strength of cross tension increases with welding time, and insensitive to the change of weding tool rotational speed and press depth. The joint cross section metallograph show that the joint vertical interface is the weak joining area. The microhardness distribution indicates that the joint weak microzone locates in joint horizontal interface.

Key words: refill friction spot welding; aluminium-lithium alloy; mechanical properties; microhardness

Shakedown analysis of U-groove butt welded joints under cyclic thermo-mechanical loadings ZHENG Xiaotao, PENG Changfei, YU Jiuyang, WANG Chenggang (Wuhan Institute of Technology, School of Mechanical Engineering, Wuhan 430205, China). pp 39 – 42

Abstract: The shakedown behavior of U-groove butt welded joints under cycle thermo-mechanical loadings was studied by ABAQUS according to the nonlinear superstition method. The effect of the geometrical scale of welding line, yield stress, thermal expansion coefficient and Young's modulus of the base material and weld material as well as the thickness of piping on the shakedown behavior were studied. Results showed that the geometry of welding line has little influence on the shakedown region, while the difference between the yield stress, thermal expansion coefficient and Young's modulus of the base material and welding material influence the shakedown behavior significantly due to the great local stress. Lastly, the shakedown estimation method of U groove butt welded joints was developed for engineering designs.

Key words: shakedown; welded joints; pressure piping; thermo-mechanical loadings

Microstructure and mechanical properties of floating bobbin friction stir welded joints in aluminum alloy DONG Jihong[1,2], DONG Chunlin[2], MENG Qiang[2], LUAN Guohong[2], JIAO Xiangdong[3] (1. Beijing University of Chemical Technology, Mechanical and Electrical Engineering Institute, Beijing 100089, Chian; 2. Beijing Aeronautical Manufacturing Technology Research Institute, Aviation Industry Corporation of China, Beijing 100024, China; 2. Beijing FSW Technology Co., Ltd, Beijing 100024, China; 3. Beijing Institute of Petro-chemical Technology, Beijing 102617, China). pp 43 – 46

Abstract: Microstructures and mechanical properties of the whole specimen in the 12 mm thick plate joint obtained by floating bobbin friction stir welding (FBFSW) were studied. The results showed that refined equiaxed grains could be observed in weld nugget zone (WNZ), and the segregation phases were broken up and mostly dissolved into the matrix. The microstructure in the heat affected zone (HAZ) consists of coarse bar-shape recovery grain. The profile of micro-hardness across the weld exhibits like "W" and the fluctuation in hardness along the thickness direction of joint was small and that the HAZ has serious softening. The fracture analysis showed that the fracture mode of the joint is ductile fracture. When the rotating speed is 600 r/min and the wielding speed is 300 mm /min, the good weld is achieved. The tensile strength of the joint reaches 231 MPa, which is about 79% of the ultimate strength of the base material.

Key words: floating bobbin FSW; microstructure; mechanical properties; 6082 aluminum alloy

Ultrasonic-assisted brazing of Al/Fe with Al alloy WANG Qian, LENG Xuesong, YAN Jiuchun, CHENG Xianoguang (State Key Laboratory of Advanced Welding and Joining, Harbin Institute of Technology, Harbin 150001, China). pp 47 – 50

Abstract: Al/Fe clad materials joining with Al alloy were successfully realized at intermediate temperature without flux in air by using ultrasonic-assisted brazing. Mechanical properties and microstructure of joints with Zn-Al and Al-Si filler metals were studied. The experiment showed that the oxide film of Al film at clad materials were effectively removed when Al/Fe clad materials were brazed with 5A06 alloy by using Zn-Al filler metal. Diffusion of Al film was easily controlled. There were not Fe-Al intermetallic compounds in the joins. Shear strength of joints was higher than 70 MPa when the Al film was not completely dissolved. The joints were composed of α-Al, η-Zn, Zn-Al eutectic and Zn-Al eutectoid. When Al/Fe clad materials were brazed with 1100 Al by using Al-Si filler metal, the Al film was completely dissolved in a short time. Fe-Al-Si intermetallic compounds and microcracks were observed and the shear strength was only 20 MPa.

Key words: ultrasonic-assisted brazing; Al thin film/Fe clad materials; Al alloy; Zn-Al filler metal; Al-Si filler metal

Microstructural characteristics and mechanical properties of laser-welded copper and aluminum XUE Zhiqing[1,2], HU Shengsun[1,2], ZUO Di[2], SHEN Junqi[1,2] (1. Tianjin Key Laboratory of Advanced Joining Technology, Tianjin University, Tianjin 300072, China; 2. School of Materials Science and Engineering, Tianjin University, Tianjin 300072, China). pp 51 – 54

Abstract: Microstructures of laser-welded Cu-Al joint are different from that made by other welding methods due to the rapid heating and solidification during laser welding process, which produces the high temperature and constituent gradient in the welding pool. In present paper, laser lap welding of copper and aluminum, tensile shear testing, examinations of weld joint cross-section and fracture surface using SEM & EDS were carried out to study the microstructural characteristics of laser-welded Cu-Al joint and the effects of microstructure on the joint mechanical properties. The results show that diverse microstructures were formed in the joint under the conditions of high temperature and constituent gradient due to the high solidification rate of laser welding process. Several different zones were identified in this study. They are band shape hypereutectic with the characteristic of parallel arrangement, mixed structures of hypereutectic and eutectic (mixed zone for short), lamellar eutectic and dendritic hypoeutectic. The results of tensile testing and fracture surface analysis indicate that the defect occurred in the mixed zone of hy-

pereutectic and eutectic structure. With the increase of welding speed, mixed zone width decreased and the hypereutectic morphology transited from the equiaxed shape to band shape. Meanwhile, the maximum shear strength of the weld joint increased with increasing of welding speed.

Key words: laser welding; dissimilar metals; microstructure; mechanical properties

Thermal kinetics for phase transformation of CuZnSnSi alloy BAO Li, LONG Weimin, PEI Yinyin, MA Jia (State Key Laboratory of Advanced Brazing Filler Metal & Technology, Zhengzhou Research Institute of Mechanical Engineering, Zhengzhou 450001, China). pp 55 - 58

Abstract: CuZnSnSi alloy performs well on brazing steel. This paper aims at studying the thermal kinetics for the melting phase transition process with CuZnSnSi alloy as filler metal, by DSC and TG techniques and the differential and integral non-isothermal analysis methods. The results show that endothermic peak starts at 1 150.5 K and ends at 1 221.5 K. The peak temperature of heat absorption is 1 174.46 K. The endothermic peak in the heating process is lower than that in the cooling process while transforming without reaction, which indicates that undercooling is necessary to make the alloy crystallize. The calculated apparent activation energy is 615.72 kJ/mol and the transition rate varies with T as the function of $k = 1.71 \times 1\ 027\exp(-6.16 \times 10^5/RT)$.

Key words: filler metal; phase transformation; thermal kinetics; DSC technique; apparent activation energy

Effect of strain rate on mechanical behavior of lead-free solder joints AN Tong, QIN Fei, WANG Xiaoliang (College of Mechanical Engineering and Applied Electronics Technology, Beijing University of Technology, Beijing 100124, China). pp 59 - 62, 104

Abstract: Tensile properties and fracture mechanism of Sn3.0Ag0.5Cu/Cu solder joints aged at 150 ℃ for different time were investigated at the strain rates of 2×10^{-4}, 2×10^{-2} and 2 s^{-1}. Experimental results show that the strain rate plays a significant role in the strength and the fracture behavior of the solder joints. The tensile strength of the solder joints increases with increasing of strain rate. The solder joints fail in a ductile mode within the solder at the low strain rate, but fail in a brittle mode inside the IMC layer at the high strain rate.

Key words: solder joint; intermetallic compound; strain rate; tensile strength

Research on decoupling of trajectory error compensation for multi-joint welding robot LI Xueqin[1], JIANG Honghai[2], YIN Guofu[1], HU Xiaobing[1] (1. School of Manufacturing Science and Engineering, Sichuan University, Chengdu 610065, China; 2. School of Electrical and Mechanical Engineering, Kunming University of Science and Technology, Kunming 650504, China). pp 63 - 66

Abstract: Because of the influence of different error sources, the end of the welding gun doesn't follow predefined trajectory. An additional movement approach was presented to compensate position and orientation errors for each joint of the welding robot which caused small perturbation on the welding gun so that the error was eliminated. Since there were serious coupled interactions between kinematic pairs of the joints of 6-DOF welding robot, error compensation model was established based on small error assumption by analyzing the relationship between the robot coordinate system. The value of error compensation for each joint of the robot can be calculated accurately through the mathematical model. The correctness of decoupling methods and modeling presented in this paper were verified by the simulation analysis. The results showed that the algorithm can effectively reduce the position and orientation errors for the end of welding gun, which offered an effective theory foundation for the control of the pose accuracy in the welding robot.

Key words: welding robot; decoupling; error compensation; accuracy

A seam tracking method for overlap sheet welding based on magnetic-control arc sensing HONG Yuxiang, XIANG Xiaoming, HONG Bo, HE Rongtuo (School of Mechanical Engineering, Xiangtan University, Xiangtan 411105, China). pp 67 - 70

Abstract: The automatic seam tracking of overlap seams of sheet was always a particular problem in the welding field. According to the characteristics of its welding procedure, a seam tracking method for overlap sheet welding based on magnetic-control arc sensing is proposed in this paper. By employing external alternating transverse magnetic field to control arc motion, this method acquires the real-time welding deviation through detecting the variation rules of welding currents. Wavelet threshold de-noising method is selected to process the current signals after contrastive analysis on the filtering results of the two-level second-order Butterworth filter and the wavelet filtering. Based on the analysis of characteristics of overlap sheet welding and the motion of magnetic-control arc, a control method of welding deviation correction based on the combination of unilateral-compared midpoint-divided area integral method and the torch-control method is proposed. The results of practical seam tracking experiments demonstrate that the automatic seam tracking method proposed can effectively resolve the dilemma of real-time seam tracking during overlap sheet welding.

Key words: overlap sheet welding; magnetic-control arc sensing; wavelet filtering; unilateral-compared midpoint-divided area integral method

Numerical simulation of resistance spot welding considering phase transition effect YI Rongtao, ZHAO Dawei, WANG Yuanxun (Hubei Key Lab for Engineering Structural Analysis and Safety Assessment, Huazhong University of Science and Technology, Wuhan 430074, China). pp 71 - 74

Abstract: The thermal expansion works in the whole welding process. Taking into account the phase transition on the thermal expansion coefficient, a two-dimensional axisymmetric finite element numerical analysis model of the resistance spot welding considering the effects of phase transition was performed. Then based on the thermal results considering the impact of latent heat, the resistance spot welding stress field and deformation of the weldment of dual-phase steel DP600 were analyzed with the thermal elastic-plastic theory and the linear rule of mixtures taking into account of the phase transition. The results